3D Model for Atomic Sputtering of Heterogeneous Ceramic Compounds

Aaron M. Schinder[1], Mitchell Walker[2], and Julian J. Rimoli[3]
Georgia Institute of Technology, Atlanta, GA 30332 USA

The erosion of the channel wall in Hall effect thrusters (HETs) limits the maximum HET operating life time. HET channel wall materials are often binary composites of boron nitride and silica. The heterogeneity of the material drives the development of complex surface features and roughness during the erosion process. To aid the understanding of the erosion processes, a three dimensional model of the atomic sputtering of a heterogeneous material is developed. The model investigates, through a ray-tracing technique and empirical models for the erosion rate of each phase, the interaction between ion beams and the underlying grain-level microstructure. Simulated erosion histories and surface profiles are compared with empirical data collected from the eroded channel wall of the AFRL/UM P5 HET. Simulated surface features and expected surface roughnesses for moderate ion incidence angles of 30˚ and 45˚ resemble those found through scanning electron microscopy and optical profilometry of the P5 channel wall. Predicted rms roughnesses for 30˚ incidence are on the order of 7 µm, and rms roughnesses measured on the channel wall are 6±2.5 µm. The composition of the channel wall surface is investigated via X-ray photoelectron spectroscopy and is comparable to prior work, but the reduction in the presence of BN with erosion is not adequately captured by this model.

Nomenclature

B_i	=	angle function fitting parameters
E_{th}	=	threshold energy for sputtering (eV)
$f_{v_i}(v_i)$	=	distribution function for single velocity component
$f_v(\vec{v})$	=	distribution function for ion velocity
gx, gy	=	average slope in x and y
k	=	sputtering rate scaling parameter
k_b	=	boltzman's constant
$\hat{n}$	=	node surface normal vector
T	=	effective ion temperature
$v_{center,i}$	=	component of the mean or bulk velocity of the plasma
Y	=	sputtering yield for a given incidence angle and impact energy (mm^3/C)

I. Introduction

Hall effect thrusters (HETs) are attractive candidates for many space propulsion applications including satellite stationkeeping. HETs typically operate at specific impulses of around 1300 s at a higher thrust-to-power ratio than gridded ion engines. Recent qualification life testing of the BPT-4000 HET demonstrated operation of the thruster for 10,400 hours[1,2]. One of the limits to HET lifetime is the erosion of the discharge channel wall materials by the plasma. Figure 1 shows a cross-sectional diagram of a typical HET discharge channel, displaying the channel wall, magnet material, and region of interest for erosion. The ceramic discharge channel wall of the HET protects the magnetic circuit from the energetic plasma. Accelerated ions erode the discharge channel wall over the operational life of the thruster, eventually exposing the magnetic circuit to the plasma. The erosion of the magnetic circuit alters the magnetic field topology, which changes the performance of the HET. After the ferrous magnet

[1] Graduate Student, Aerospace Engineering, 270 Ferst Dr NW, Full Member AIAA
[2] Associate Professor, Aerospace Engineering, 270 Ferst Dr NW, Associate Fellow AIAA
[3] Assistant Professor, Aerospace Engineering, 270 Ferst Dr NW, AIAA Member

material begins to sputter, the ejection and subsequent redeposition of the metal onto the spacecraft structure can destroy electrical isolation and degrade the performance of other hardware.

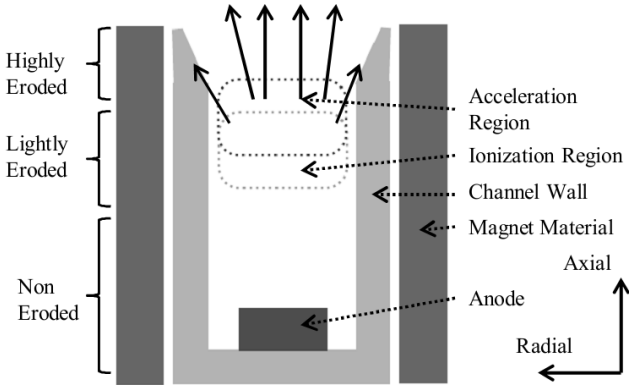

Figure 1. Erosion process in HET discharge channel

In a HET, gas enters the discharge channel through the anode gas-distributor. The neutral gas travels through the channel until it reaches the energetic cloud of electrons trapped by the radial magnetic field near the exit plane of the channel. The gas is ionized by the electrons and then accelerates across a narrow potential drop (*i.e.*, a few millimeters wide) to a high velocity, at which it is exhausted from the thruster. The erosion in the discharge channel occurs primarily in the region immediately downstream of the accelerating potential drop.

A. Current Erosion Modeling

In order to predict design life, erosion models based on theoretically atomic sputtering mechanism are employed. The current state-of-the-art in the prediction of channel wall erosion involves the use of two-dimensional empirically or numerically derived atomic sputtering models, as well as axisymmetric two-dimensional simulations of the plasma, to produce profiles of the average discharge channel wall radius as a function of axial position. Software tools such as HPHall and 1dhydro can be used to perform erosion analysis given a material model[1,3,14]. However, these erosion models have three inherent limitations.

The first limitation of present erosion models is that the experimental data that they are derived from is from experiments conducted with little data below 250 eV[8]. In the low discharge voltage modes of HET operation, ion energies of 100-300 eV are present. Thus, the modeled material response to the lower energy portions of the ion energy distributions is not well supported by experimental data.

The second limitation of present erosion models is that they treat the material as a homogenous isotropic solid.[3] Consequently, these models do not adequately capture the behavior of the material surface roughness nor explain features that can develop during thruster operations (e.g., the saw-tooth erosion ridges observed during the qualification life testing of the BPT-4000 thruster shown in Figure 2)[2]. Current erosion models can only capture an average of the erosion depth, not the full geometry of the erosion grooves or surface composition.

The third limitation of present models is that axisymmetric and 2D models cannot capture the inherently 3D nature of the surface roughness. 2D models treat any surface that results from erosion as a body of rotation, losing any data about azimuthal structure.

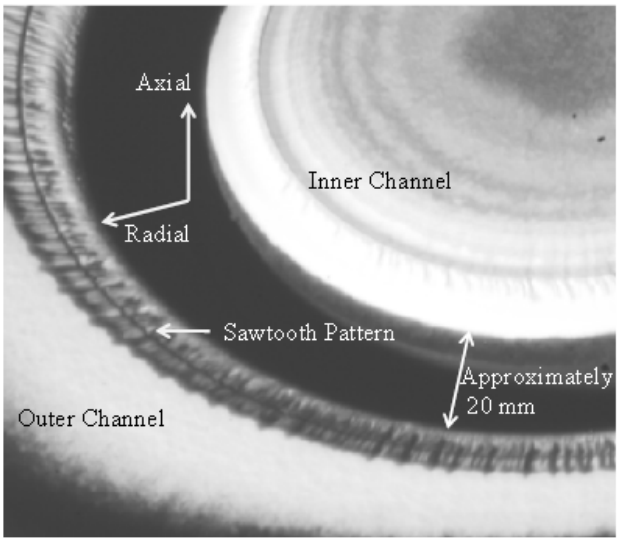

Figure 2. BPT-4000 channel wall erosion after 10,400 hrs[2]

B. P5 Channel Wall Erosion Study

In order to develop a better understanding of the physics and important processes of channel wall erosion, the channel wall of the AFRL/UM P5 HET was investigated using scanning electron microscopy (SEM), X-ray photoelectron spectroscopy (XPS) composition measurements, and optical profilometry. The P5 was operated for more than 1500 hrs at the University of Michigan. It was operated at power levels of 1.6, 3, and 5 kW under a variety of discharge voltages and flow conditions, as described in the thesis work of Haas, Gulczinski, and Smith. Table 1 presents a summary of the operating conditions[11,12,15].

Table 1. Summary of AFRL/UM P5 operating conditions[11,12,15]

Gulczinski			
Run Condition	Discharge Voltage (V)	Discharge Current (A)	Total Flow Rate (sccm)
Condition 1	300	5.3	64
Condition 2	500	5.3	64
Condition 3	500	10	111
Haas			
Run Condition	Discharge Voltage (V)	Discharge Current (A)	Total Flow Rate (sccm)
Condition 1	300	5.3	63
Condition 2	300	10	63
Smith			
Condition 1	300	5.3	61
Condition 2	300	10.4	114

Haas and Gulczinski measured the plasma number density profiles and ion energy distributions under these operating conditions. At the 1.6-kW run condition analyzed by Haas, xenon ion number densities were given between $2x10^{17}$ and $6x10^{17}$ m^{-3}, and at the 3-kW condition, the ion number densities were between $6x10^{17}$ and $1x10^{18}$ m^{-3}.[11] Gulczinski also measured numerous ion energy distribution functions within and around the channel; at the 1.6-kW run condition the ion energy distribution function centers around 250 eV with roughly a 50-eV full-width at half-maximum.[12] In order to simulate conditions relevant to the environment to which the channel wall has been exposed, the experimental data described above are used to define the plasma properties in the numerical model described in Section II.

The channel wall of the P5 HET is composed of Combat M26-grade BN-SiO_2. Common materials used for HET discharge channel walls are boron nitride and silica composites (e.g., Combat M and M26) because of their superior machinability and ease of forming over pure BN grades like A and HBC. The composite is not an isotropic material;

in grade M26 (60% BN and 40% silica by mass) highly irregular BN grains are on the order of tens of micrometers wide by hundreds of nanometers thick. These grains are interspersed in a silica matrix, which has large domains of relatively pure silica about 20 μm across. Such microstructures are visible in SEM images of the channel wall, as shown in Figure 3.

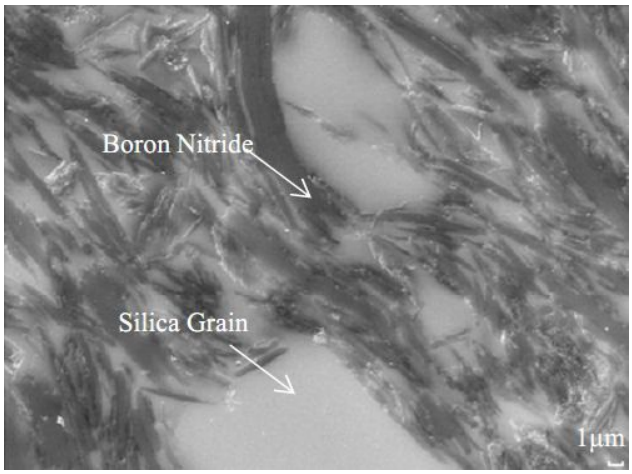

Figure 3. Cross-sectional SEM of M26 BN-SiO_2 composite

Surface profiles of the channel wall surface were taken with an Olympus-LEXT 3D confocal microscope. Three regions of interest were investigated, differing by the degree to which the surface was eroded by contact with the plasma. The regions were termed the non-eroded, lightly-eroded, and highly-eroded regions. XPS spectroscopy yielded information about the surface composition in the three regions. Excerpts from these data are compared with the heterogeneous numerical model in Section IV.

II. Model Overview

A. Heterogeneous Model

To simulate the erosion of the channel wall material in greater detail, a three-dimensional model of the sputtering of a binary material has been developed. This 3D model reproduces some important features of the surface structures that were found in measurements of the eroded P5 channel wall, and the model provides insight into how a heterogeneous material drives the formation of 3D surface roughness and geometry.

In the present approach, ray-tracing techniques are used to determine the regions of the material surface that are exposed to ion bombardment, or shadowed. In the present approach, each material phase has its own atomic sputtering model, which returns the sputtering yield as a function of impact angle and energy. Both BN, and SiO_2 exposed surfaces have a separate angle and energy dependence to their yield functions and erosion rates. The ion impact angles are calculated based on the local incidence angle of each velocity component of the plasma. Figure 4 shows the ray tracing approach.

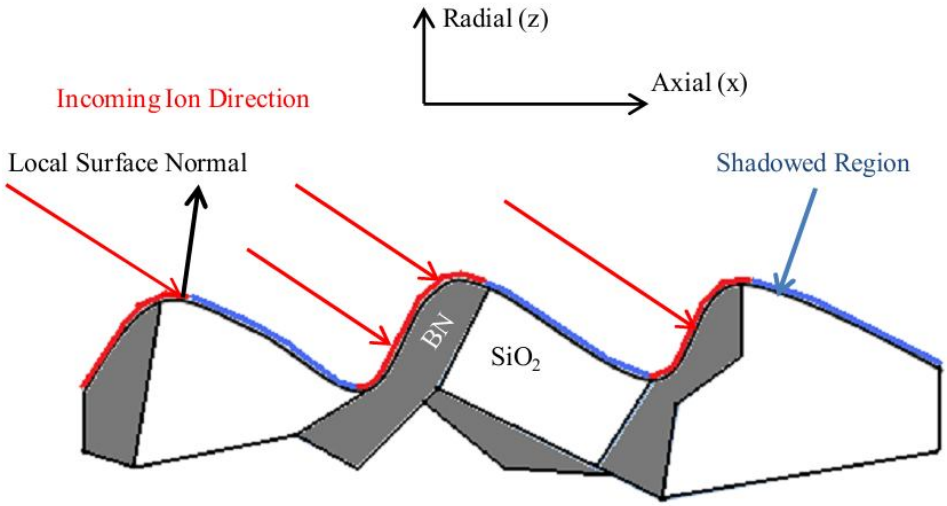

Figure 4. Ray-tracing approach to differential sputtering

A continuum model of erosion is justified, due to the scale of the atomic sputtering events and the rate at which ion impacts occur. The scale of atomic sputtering events is on the order of 1 to 10 nm, with yields of cubic nanometers or less per impact, according to the scales of atomic sputtering observed in experiments[7,8,9] and theoretical tools such as Stopping Range of Ions in Matter (SRIM)[10]. The grid spacing chosen during simulation is on the order of tenths of μm for the small-scale domain model, and 1 μm for the large scale domain model, with the impact rate on the order of 10^9 impacts/μm^2-sec.

B. Flow of Execution

The sputtering model consists of a model of the 3D material domain, a model of either an ion beam or a thermal distribution of velocities in a thermal plasma, and a model of the two-dimensional surface geometry. During the modeling of erosion, a volumetric region of material information is generated, and the surface mesh is initialized at the top of the simulation domain. For each timestep, the material type at each point on the surface is calculated, along with the local surface normals. Then, the shadowing is calculated to determine whether or not ions can impact each point on the surface. Next, the local erosion rate is calculated as a function of the material, the ion energy and direction, and the local surface normal. Finally, the surface mesh geometry is updated. Figure 5 shows the sequence of execution for the model.

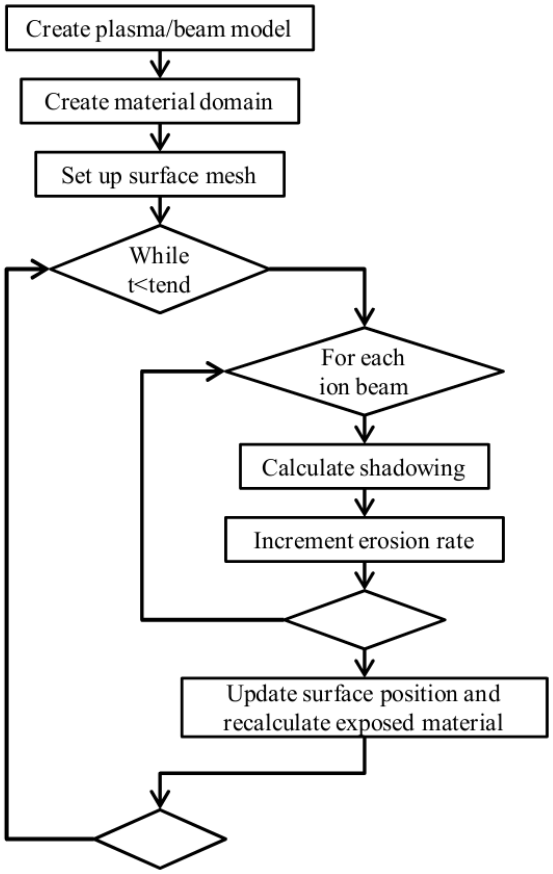

Figure 5. Sputtering model flow chart

C. Discretization Scheme

The surface is discretized as a two-dimensional regular grid. For each point on the surface, the local normal is calculated in terms of the height of the four adjacent nodes. The local surface area exposed for each node is the cell area divided by the cosine of the local surface normal angle with the vertical.

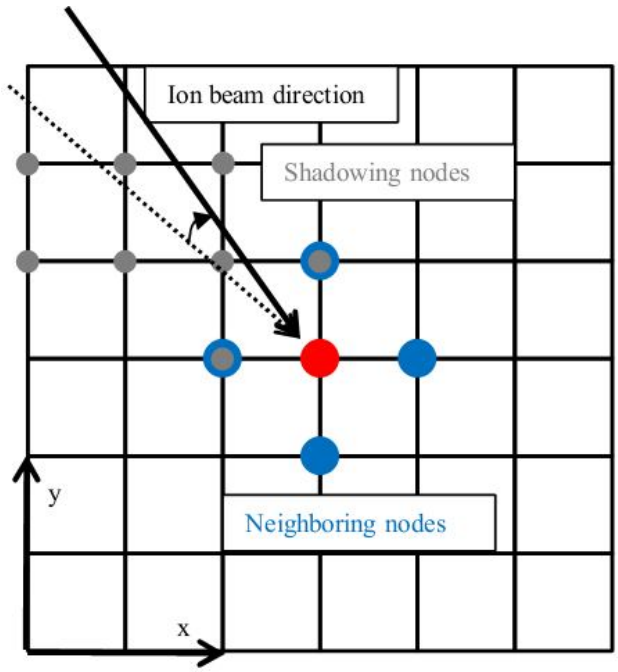

Figure 6. Surface mesh. *Blue circles are neighboring nodes for local normal calculations, grey are nodes chosen to test for shadowing of the target node for each ion beam direction*

The local surface normals are calculated as follows:

$$\begin{cases} g_x = \frac{1}{2}\left(\frac{z_{i+1,j} - z_{i,j}}{x_{i+1,j} - x_{i,j}}\right) + \frac{1}{2}\left(\frac{z_{i,j} - z_{i-1,j}}{x_{i,j} - x_{i-1,j}}\right) \\ g_y = \frac{1}{2}\left(\frac{z_{i,j+1} - z_{i,j}}{y_{i,j+1} - y_{i,j}}\right) + \frac{1}{2}\left(\frac{z_{i,j} - z_{i,j-1}}{y_{i,j} - y_{i,j-1}}\right) \\ \hat{n} = \frac{[-gx \quad -gy \quad 1]}{\sqrt{gx^2 + gy^2 + 1}} \end{cases} \tag{1}$$

During each timestep, for each ion beam direction, whether or not a given node is in shadow is calculated based on whether or not the ion beam vector intersects any triangle formed by a trio of the nodes along the line of sight of the ion beam vector. To reduce the required computational time, only those nodes along the line of sight are compared when calculating the shadowing.

D. Plasma Model

In a HET, the ions are accelerated to a high velocity in a given direction, but also have a Maxwellian distribution of speeds due to thermal motion, which can be modeled with an effective ion temperature. The simulation software is capable of modeling either single monoenergetic ion beams or a plasma with a center velocity and distribution of ion energies and directions. Single ion beams are used for moderate incidence angles, where the 5º of spread in the ion angle due to thermal motion is not significant. The full plasma case is used to model a plasma travelling parallel to the wall, with thermal motion causing drift into the wall.

The model captures the variation in ion energies and the variation in the angle at which the ions impinge on the surface by dividing a Maxwellian velocity distribution into velocity classes. A plasma mean velocity is assumed, related to the net velocity of the ions after passing across the acceleration potential drop in the discharge channel. An effective temperature for the ion energy is also assumed, chosen based on the ion energy distribution measurements in the works of Gulczinski and Haas[11,12], produces a Gaussian distribution of velocities around the center velocity. For each dimension of velocity space, the distribution is then partitioned into velocity classes. The fraction of the

total ion number density is binned for each of these velocity classes, and this fraction is normalized so that the total fraction for all bins sums to one. An ion beam structure is created for each velocity class, with the energy and direction calculated from the center velocity of the velocity class bin. Equation 2 shows the expression for a Maxwellian velocity distribution offset by a relative mean velocity.

$$\begin{cases} f_{v_i}(v_i) = \sqrt{\dfrac{m}{2\pi k_b T}} \exp\left(\dfrac{-m}{2k_b T}\left(v_i - v_{center,i}\right)^2\right) \\ f_v(\vec{v}) = \prod f_{v_i}(v_i) \end{cases} \tag{2}$$

The simulation calculates shadowing and erosion rates for each ion beam. The erosion rates are summed for a total erosion rate, and the velocities are then updated.

E. Material Domain Model

Two different material domain geometry models are used to capture features and behavior at different scales. Each model uses a different grain geometry and interprets the remaining material as a matrix. On small scales, long thin triangular BN grains are embedded in a silica matrix. At larger scales, large regions of pure silica are embedded in BN-rich regions.

A small-scale model, an example of which is shown in Figure 7, with mesh sizes on the order of tens of micrometers on a side, is intended to capture individual BN grains. The BN grains are modeled as triangular flakes interspersed in a silica matrix. The BN grains have a uniformly distributed randomized width and length scale based on minimum and maximum specified lengths and thicknesses. Lengths and thicknesses are chosen to produce material cross sections similar to those imaged experimentally. The grains are placed with a random orientation within the simulation domain until a certain volume fraction is achieved.

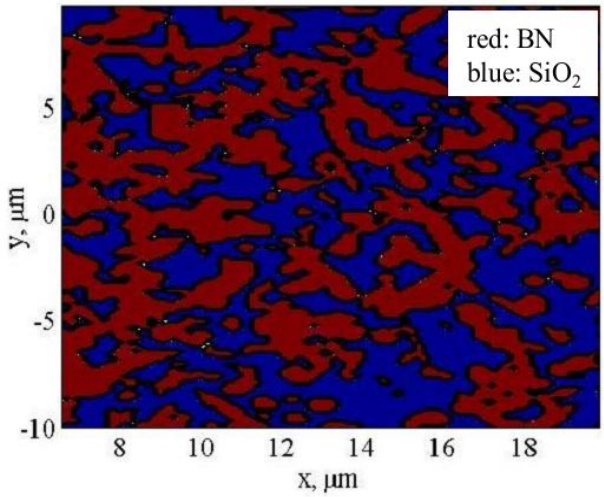

Figure 7. Small-scale material model cross section

The large scale model, with mesh sizes on the order of hundreds of micrometers, is intended to capture the larger scale surface roughness and the large silica grains. An example is shown in Figure 8. These silica grains, modeled as ellipsoidal regions, are placed randomly throughout the domain until a certain volume fraction is achieved. The interstitial area is assumed to be dominated by BN grains, although no attempt is made to resolve the individual grains.

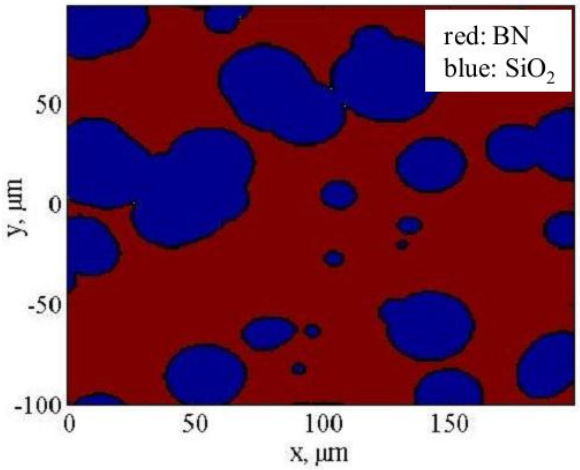

Figure 8. Large scale material model cross section

F. Component Atomic Sputtering Models

A homogenous isotropic sputtering model for M26 BN-SiO_2 is provided by Gamero-Castano, who fit his curve to experimental data collected by Garnier[8,9,14]. Curve fits of a similar form were created, for the purposes of comparison, from experimental data collected by Yalin and used as the material model for each phase, respectively. The models were fitted to the experimental sputtering data collected by Yalin *et al.* for grade HBC, an almost pure BN material, and for quartz[7] (silica). The curve fit expressions have the following form: Y is the sputtering yield in mm^3/C incident ion current, E is the impact energy in eV, E_{th} is the sputtering threshold energy, and α is the incident angle in degrees. The sputtering yield is the volume of material ejected for a given incident current, assumed to be singly ionized, in Coulombs.

$$Y(E,\alpha) = Y_E(E)Y_\alpha(\alpha) = k(B_0 + B_1\alpha^1 + B_2\alpha^2 + B_3\alpha^3)\sqrt{E}\left(1 - \sqrt{\frac{E_{th}}{E}}\right)^{2.5} \tag{3}$$

Table 2 shows the coefficients for each model. The Gamero-Castano model is an example of a sputtering model used in the literature. Yalin's HBC and Quartz models are used for the boron nitride and silica phases within the present model.

Table 2. Material model coefficients

Material	Gamero-Castano M26 (60% BN, 40% SiO_2)[14]	Yalin HBC (99% BN)[7]	Yalin Quartz (Silica)[7]
E_{th} (eV)	58.6	18.3	18.3
B_0	9.90E-03	1.18E+00	9.14E-01
B_1	0.00E+00	1.94E-02	5.34E-02
B_2	6.04E-06	1.22E-04	-6.98E-04
B_3	-4.75E-08	-2.22E-06	3.33E-06
K	1.00E+00	2.28E-03	3.50E-03

Figure 9 shows the curve fits and presents the experimental sputtering data at 45 degrees incidence angle. The curve fits are based on data at several energies and incidence angles. This one was chosen because all data sets have some data at this angle. At low ion energies < 200 eV, BN-SiO_2 is expected to have a lower sputtering yield than silica. However, according to the data collected by Garnier and Yalin *et al.*, the BN-SiO_2 material is modeled as eroding faster than the silica at high impact energies. This is not likely to be physically realistic and may be due to

differences in measurement methods for the yield, as Yalin measured erosion in an angle-resolved manner with deposition on a quartz crystal microbalance whereas Garnier measured erosion with a net mass loss after a period of exposure.

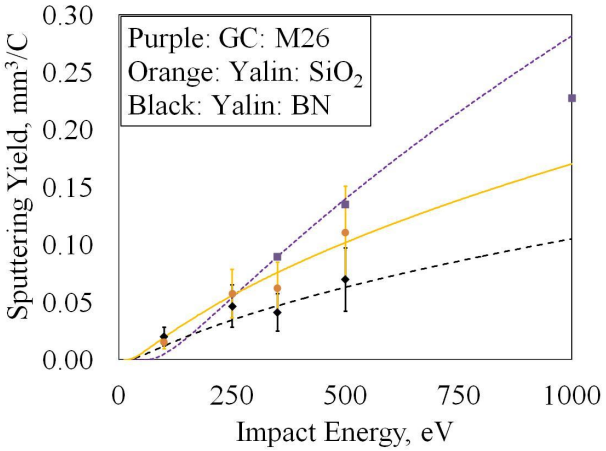

Figure 9. Curve fits to sputtering data, 45 deg incidence

G. Analysis of Simulation Convergence

A convergence study is conducted at both small-scale and large-scale domain sizes to confirm the numerical stability of the simulation. Numerical instability and divergence of the results were found to occur for large time steps, originating in areas of large curvature. The instabilities took the form of ripples which propagate from these areas. If the ripples are large enough, they interact significantly with the shadowing, and instability results. This effect is exacerbated at shallow incidence angles, so shallow incidence angles were used as the limiting case for the convergence study. Table 3 shows the run conditions of the convergence study.

Table 3. Convergence study run conditions

	Small Domain Study	**Large Domain Study**	
Domain Size	30 x 16	200 x 100	μm
Mesh	400x200	200x100	
Material:	BN Flakes	Ellipsoidal Silica Grains	
Min length scale	3	0.1	μm
Max length scale	10	10	μm
Min radius scale	0.1	5	μm
Max radius scale	0.4	20	μm
BN volume fraction	0.6	0.6	
Ion Beam:			
Ion energy	245.6	245.6	eV
Incidence Angle	1.5˚	5˚	
Number Density	3E+17	3E+17	m^{-3}

For the small domain study, the average erosion rate came to within 5% of the asymptotic value at a timestep of 2 seconds, and the rms roughness of the produced profiles converged. For the large domain study, the average erosion rate approached 0.5% of the asymptotic value at a timestep of 2 seconds. Figure 10 shows the convergence of the average erosion rates. These timesteps were used in subsequent simulations at these relative mesh sizes.

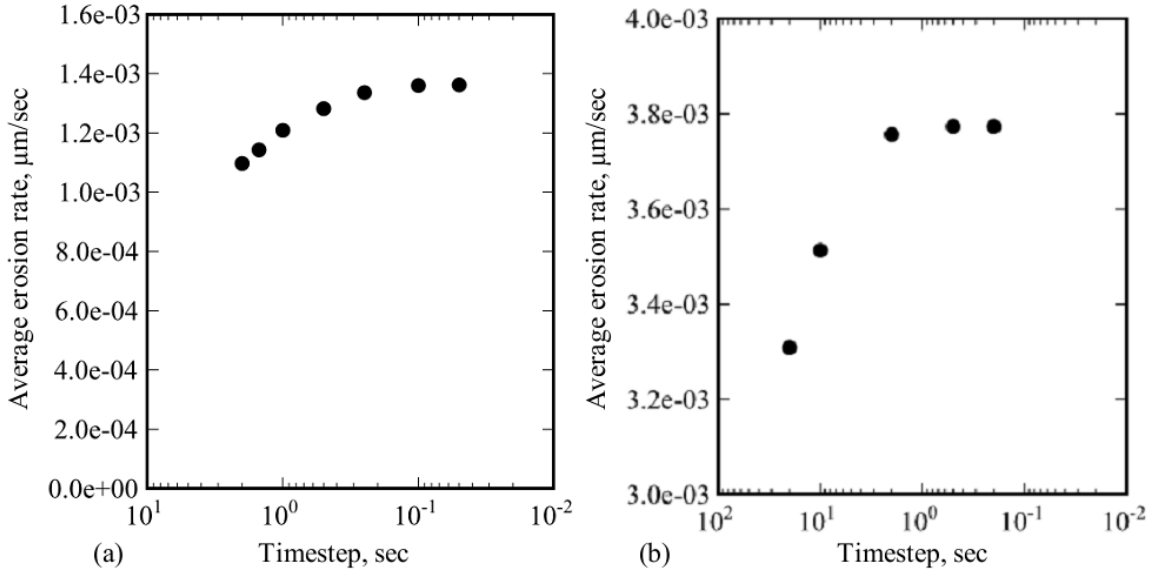

Figure 10. Convergence of average erosion rates - *a) small-scale domain model b) large-scale domain model*

H. Verification of Implementation

In order to confirm that the behavior of the model is physically reasonable, and related to the more basic component models for each phase, several large-scale material domain models are generated. Each material domain model has a different silica volume fraction, ranging from 0% (no silica grains) to 100% silica. The incidence angle of the ion beam is set at 30 degrees. It is expected that the behavior of the model is identical to that of the component models when only that material is present. No surface features should form, as the erosion rate is constant across the entire surface.

In addition, the average rate of erosion should be a smooth function of the fraction of the surface composed of each material. The surface features may modify this with the angles with which the ion beams strike the bumps, but it should be a smooth function on average. Figure 11 shows the average erosion rates produced by the models . In the limiting case where the boron nitride fraction is 100%, no surface roughness or features are produced, *i.e.* the simulation produces a flat surface for each timestep, and the recession rate agrees exactly with the component model for BN.

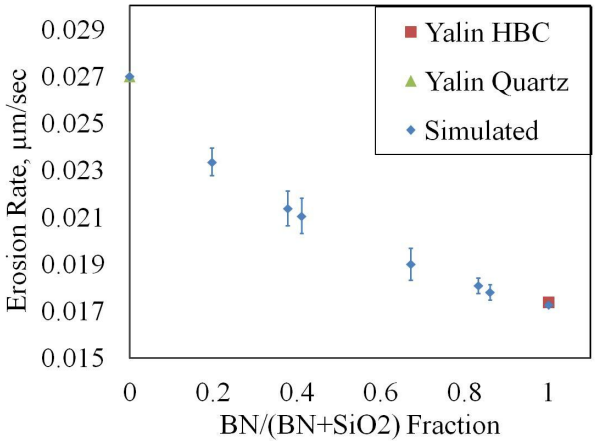

Figure 11. Average and one standard deviation of erosion rate with BN fraction: Comparison with component models

The trend of the series of simulated average erosion rates is bracketed by the component models, and varies smoothly from 0 to 1. The reproduction of the component model behavior in the limits of composition, and well behaved solutions in between are taken as verification of our implementation of the two-phase model.

One aspect of the behavior of the composition series is that the average erosion rate deviates from a linear relationship between the erosion rates of the two pure-substance models. A linear relationship would be expected of a simple rule of mixture for the exposed material. This extra behavior is an effect of the developing surface structures, and highlights the need for explicit models that capture heterogeneous features.

III. Numerical Results

The small-scale material domain model produced profiles similar to the tenth-micrometer erosion striations seen in close-up SEM imagery of the P5 channel wall surface as seen in Figure 12. Ion flow at shallow incidence angles produces long thin streak-lines. Cases where the flow is locally parallel to the larger scale structure appear to produce these.

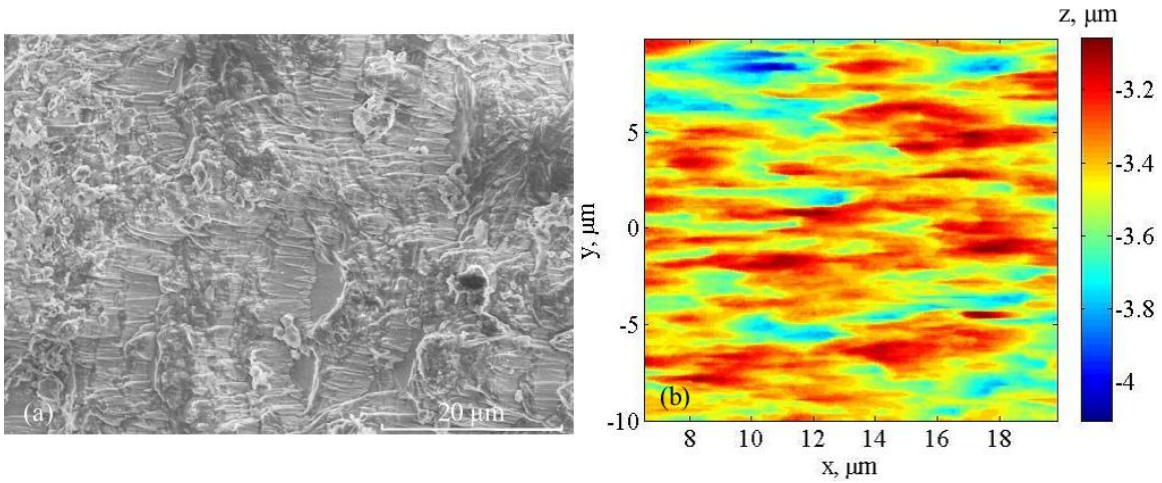

Figure 12. Comparison of SEM image with shallow-angle small domain simulation
a) SEM image of highly eroded P5 channel wall, b) Small scale simulation, 20º incidence, 750 s, 10^{17} m^{-3}, showing similar streak-like patterns

The large-scale material domain models provided the most features for comparison with our experimental data from the channel wall. Single ion beam models were used at several angles of attack to the simulated material

domain. A thermal distribution of ion beams for a full plasma was used to model a 0˚ incidence case, and 30˚ for comparison with the single ion beam case. Table 4 lists the conditions for the large domain simulations.

Table 4. Run conditions, large-scale simulations

Domain	400x200 μm
Mesh	400x200
Material	Ellipsoidal Silica Grains
Min length	0.1 μm
Max length	10 μm
Min radius	5 μm
Max radius	20 μm
BN volume	0.6
Ion Beam Properties	
Ion Energy	250 eV
Angles	[5°, 10°, 15°, 20°, 30°, 45°, 90°]
Number Density	3.00E+17 m^{-3}
Plasma Properties	
Ion Temperature	8000 K
Ion Center Velocity	19000 m/s
Angles	0, 30°
Number Density	6E+17 m^{-3}

It was found that the distribution of the ion beams at center energies and spread similar to those indicated in the Gulczinski thesis, 250-eV run condition does not differ significantly from the single ion beam case at 30˚. The effect of the thermal distribution is most pronounced at shallow incidence angles.

The surface profiles of the simulated regions show the following in terms of erosion rate as a function of angle: The average erosion rate quickly approaches a steady state value which persists through the entire evolution of the surface profile, with only minor variations, as shown in Figure 13.

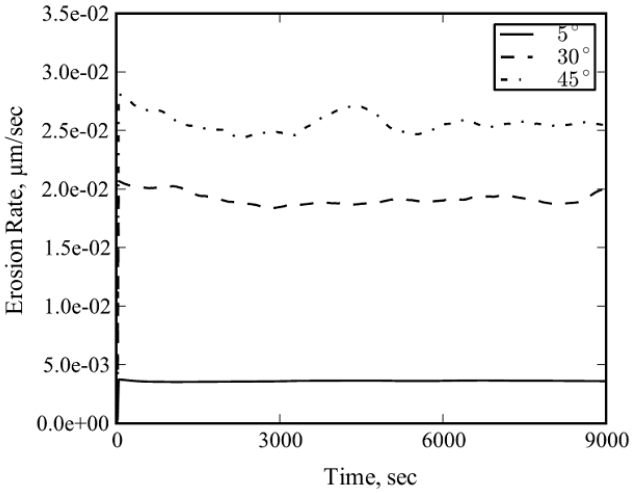

Figure 13. Average erosion rate vs. time, by incidence angle, large scale

The surface profiles of the large scale angle series are not uniform, and develop over time. Eventually, the qualitative nature of the surface appears to remain unchanged after erosion depths of ~200 um. Materials with lower sputtering yields protrude from the surface at various places, and erode away, but the relative magnitude of the features appears stable. The rms roughness of the surface continues to increase throughout the simulated time span, albeit with an apparent logarithmic or asymptotic slowdown as time advances, corresponding to the mature surfaces. The magnitude of the rms roughness profile that develops, along with the nature of the surface features, is a strong function of the incidence angle of the ion beams.

For example, each of the angle series simulations was run for 18000 s of simulated time. The 5º case achieved a shallower depth at the end of the simulated period. Figure 14 shows the rms roughness achieved at three ion beam incidence angles as a function of erosion depth.

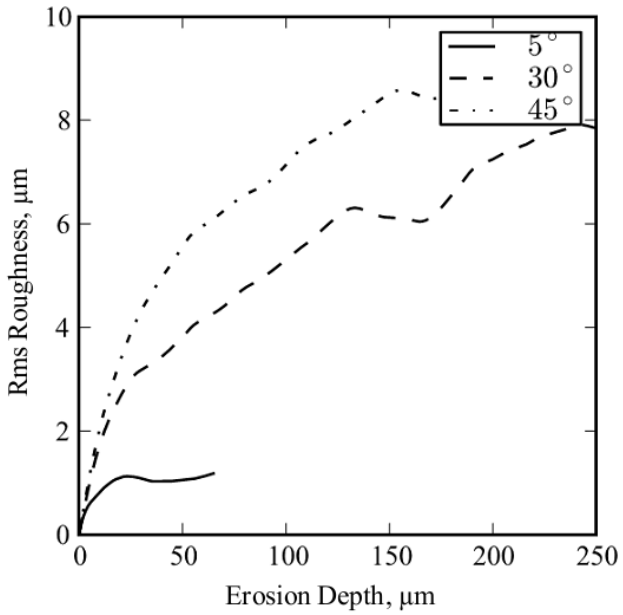

Figure 14. Rms roughness as a function of erosion depth, large-scale

A 24000 s simulation with a coarser grid and larger domain is run at 30º incidence to investigate the boundedness of rms roughness for long erosion times, shown below in Figure 15. At 470 µm erosion depth, the rms roughness is still below 9 µm and is comparable in magnitude to the results from the finer large-scale simulation (Figure 14). The peak-to-valley roughness has not yet reached a limit at 470 µm, pointing to the development of larger scale structures as the simulation advances.

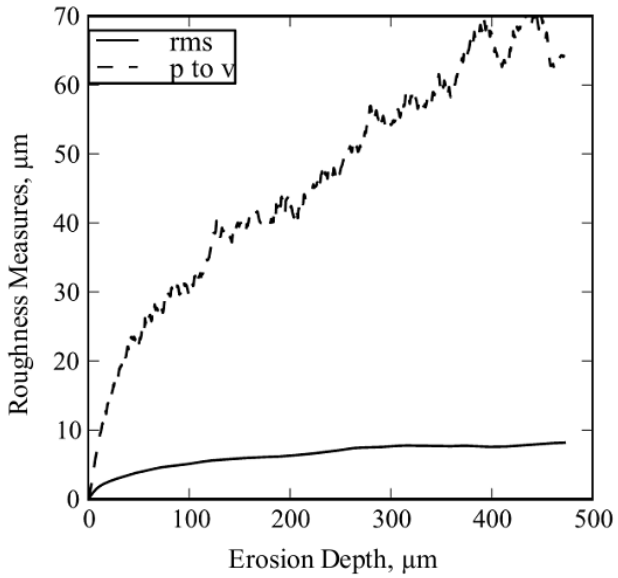

Figure 15. Rms, peak-to-valley roughness, 30°, coarse large-scale simulation

The relative presence of BN relative to SiO_2 is quantified in terms of the proportion of upward-facing area on the simulated domain as a function of time. The evolution of the BN/SiO_2 ratio is shown below in Figure 16. The ratio appears to increase from 60% to around 70% of the exposed area. The surface BN/SiO_2 ratio remains within 10% of the starting value, the average volume fraction in the material, with no coherent trend up or down as the material erodes.

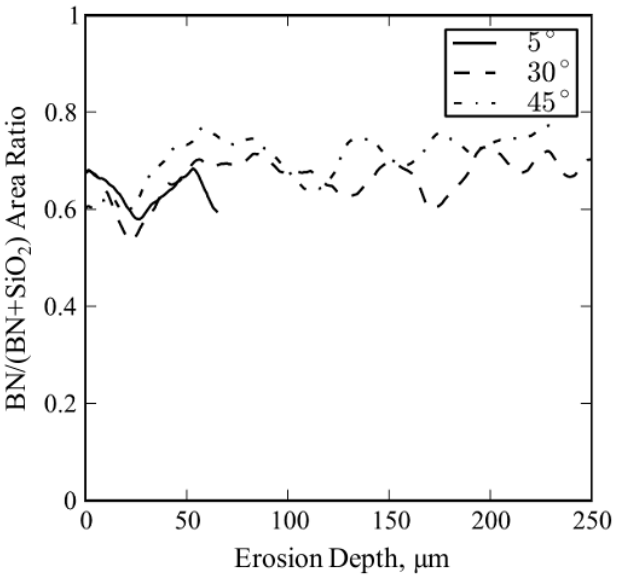

Figure 16. $BN/(BN\text{-}SiO_2)$ surface area ratio vs. erosion depth, large-scale

IV. Discussion

The P5 channel wall experimental surface characterization provides us with experimental data on surfaces eroded by HET plasma. The data is from a single point in time, but features of interest can be compared with the behavior of the model. Measurements of the surface profile, surface roughness, and surface composition can be compared with from the results of this model.

The first observation from the model behavior is that surface structures are only generated due to atomic sputtering when there is heterogeneity to the material. In Figure 11 the pure BN and pure silica models produce flat surfaces which erode at a rate exactly mirroring that of the pure component sputtering models. In simulated cases where the erosion is allowed to proceed past the defined material domain, into a region of pure material, any surface structure which is produced begins to decay back into a flat surface.

The average erosion rate of the surface is between that of the two component atomic sputtering models, as shown in Figure 11 and Figure 17 . However, the variation of the average sputtering rate with mixture fraction is not the linear law-of-mixtures that is expected from a flat featureless surface. This demonstrates the effect of surface structures in perturbing the average erosion rate. Due to the shadowing effect, the average erosion rate is closer to that of the slower sputtering material than would be expected from a linear law of mixtures.

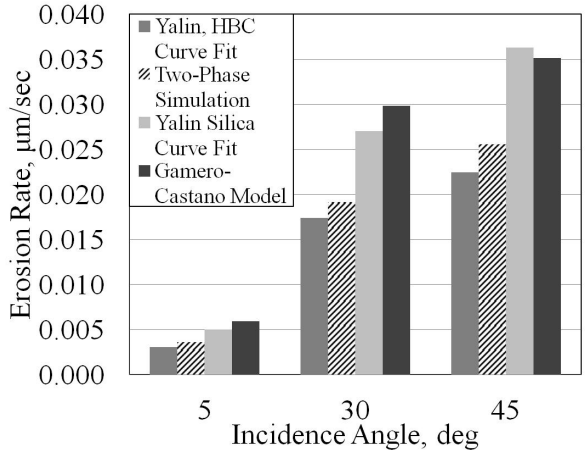

Figure 17. Comparison of single phase models to two-phase behavior

The two-phase simulation erosion rates are bracketed by the erosion rates of the constituent material models, and compared to Gamero-Castano's homogenous model for M26. These rates are for a 250 eV ion beam, $3*10^{17}$ m^{-3} xenon

Figure 15 shows that the model produces surfaces that are qualitatively mature after erosion depths are achieved on the order of a few times the length of the largest grain features. Local variations in mesh height and feature size appear to approach a steady state, as does the rms surface roughness. Peak-to-valley roughness, which is sensitive to the largest surface features generated continues to increase, even after long simulation times and 470 µm erosion depths. This suggests that with larger domains and longer times, larger scale surface features may result from the continued operation of the model.

The second main observation from the model behavior is that surface structures observed in SEM imaging of the eroded P5 channel wall are reproduced in the heterogeneous erosion model under certain beam and plasma conditions. The nature of the features produced by the erosion model are highly dependent on the angle at which the ion beam/ion beams impinge on the surface of the material.

SEM imaging of the highly eroded surface shows cliff-and-ridge structures on the order of 20 µm wide and 20-40 µm long. Contrast on the secondary electron emission shows higher BN concentrations near the front of these structures. The large scale runs also produce similar structures, resulting from the boron nitride shadowing the softer silica grains behind them. The BN ridges shield the silica cliffs from the bulk of the incoming ions. This is shown in Figure 18.

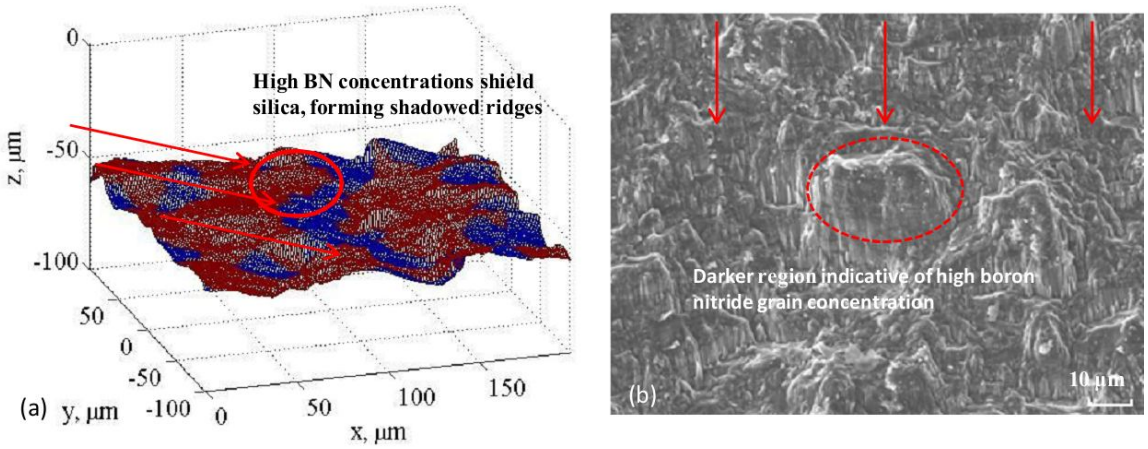

Figure 18. a) Simulated erosion profile, b) SEM image of highly eroded section of channel wall.
Image a) demonstrates the behavior of the two-phase material model. This is for an incidence angle of 30°, 3E17 m^{-3}, 750 s simulation. Regions of high BN concentration shadow the softer silica material behind the ridges, giving rise to features that appear similar to the experimental surface profiles imaged via SEM from the P5 channel wall.

These cliff-and-valley structures are also comparable in horizontal and vertical magnitude to those seen during profilometry of the eroded channel wall samples. An Olympus LEXT 3D confocal microscope is used to produce surface profiles of each of the three regions of interest on the samples. In the highly-eroded region, the scales of the eroded features in the profiles are similar to those produced by the 30˚ and 45˚ incidence angle simulations.

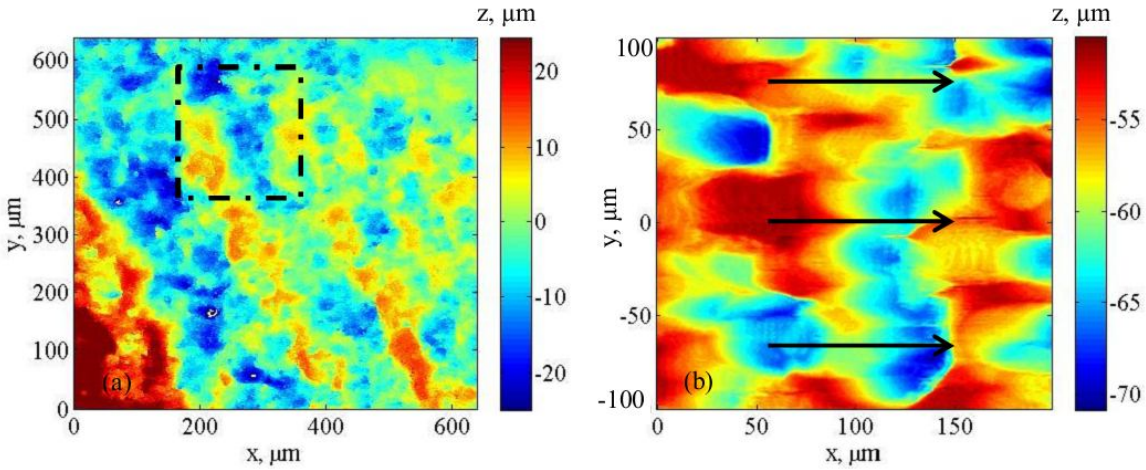

Figure 19. a) Optical profile of P5 channel wall, b) Simulated profile, 30° incidence, 750 s, 3E17 m^{-3} xenon
Image a) is an empirical profile of the highly eroded region of the P5 thruster channel wall. A region of similar size to the simulated domain is outlined for comparison. Image b) demonstrates the similarity in the peak-to-valley depth and feature size developed in the simulation.

The profilometry of the highly-eroded surface indicates an empirical rms roughness of around 6±2.5 µm. This is similar to where the rms roughness of the 30° simulated case appears to asymptote (Figure 16). The simulated roughness developed is a function of the largest heterogeneous surface features; in the case of the large-scale material domain model, the 20-µm silica grains govern the erosion.

Not all incidence angles produce surface features and roughnesses comparable to what we see experimentally. Normal incidence angles produce vertical shapes where the harder to sputter material protrudes from the softer silica materials. At parallel incidence angles, the simulated surface is only very slowly eroded, and the aspect ratios of the structures produced tend towards being semi-infinite. This produces a very smooth, polished surface.

In the plasma simulation cases when parallel center velocity is assumed, the thermal energies suggested by Gulczinski's ion energy distribution functions produce distributions of ions which impact the wall at less than 5º incidence angle. Simulations including the full plasma model do not produce erosion patterns that are significantly different from cases where a single ion beam at a shallow incidence angle is used.

Haas's plasma potential contour measurements in the P5 discharge channel suggest that the ions should experience acceleration largely along the axial direction, with little acceleration in the radial direction as expected of contemporary HET designs[11]. However, note that Haas's measurements were taken at some distance from the wall and do not account for the radial acceleration of ions due to the plasma sheath at the boundary between the channel wall and plasma.

Cross sections of the P5 channel wall have a sharp boundary between the highly-eroded and non-eroded region shown in Figure 1, corresponding to the location of the acceleration zone of the plasma. The highly-eroded region is inclined to the axis of the channel wall by about 17°, suggesting that the plasma is initially impacting the surface at a moderate incidence angle. In summary, the second observation is that we expect to see certain surface features only when ions impact at a given angle.

The third main observation concerns the composition of the eroded surface. XPS measurements are taken of the relative concentration of elements on the surface of the eroded channel wall samples. These measurements indicate that BN is depleted relative to silica in the highly eroded region of the thruster. This surprising result mirrors that obtained by Garnier in his erosion experiments on BN-SiO_2 target discs[9]. However, Zidar took energy dispersive spectroscopy (EDS) data from an eroded channel wall that instead indicated increased BN presence near the eroded end of the channel wall, differing from our results and those of Garnier[5,6]. Further investigation of the difference between our measurement results would be of interest.

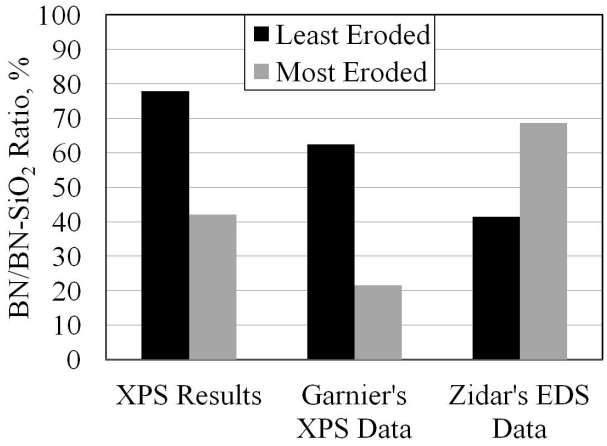

Figure 20. BN/(BN+SiO_2) ratio (percent)
XPS data from P-5 samples, Garnier's XPS data of BN-SiO_2 samples[9], Zidar's EDS data from a used M26 hall thruster[6].

The atomic sputtering model does not account for the observed changes in surface composition. Atomic sputtering alone would predict that BN would protrude from the silica matrix, and persist relative to the softer to sputter silica material. The model behavior is such that the relative amount of exposed BN increases slightly but remains within 10% of the average material in the matrix, as shown in Figure 13.

In order to illustrate the difficulty with a pure sputtering approach capturing the change in surface composition, a simple analytical model is presented. In the model, a flat surface plane propagates through a regular domain, shown in Figure 21. As the surface plane is moved into the domain, the intersection of the surface with the grains produces a similar but translated image to the initial intersection image. According to this model, the exposed area proportion of the BN grains and silica matrix should remain exactly the same. In a sputtering model, this may be modified due to exposure of the lower-yield grains, but significant variation is not observed in the present model of BN-SiO_2.

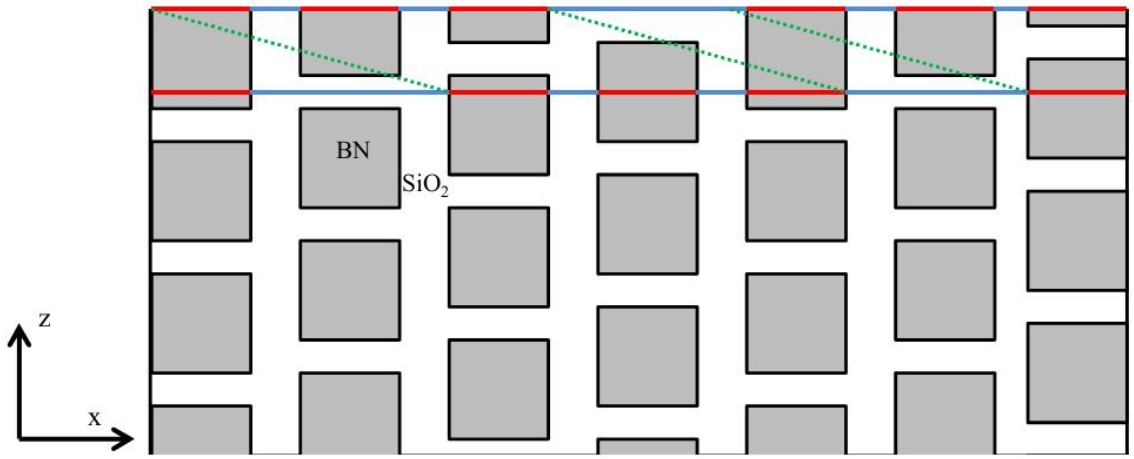

Figure 21. Simple regular domain model

If the analytical model is modified so that when a BN grains which lose a critical amount of support in the surrounding matrix are removed, it could account for changes in the silica. In this model, depicted below in Figure 22, the BN grains protrude from the matrix as it is sputtered. When the BN has a small enough supporting surface area in the silica, they are removed, leaving a shallow groove behind. In this case, the upward facing area due to silica increases after BN grains are removed.

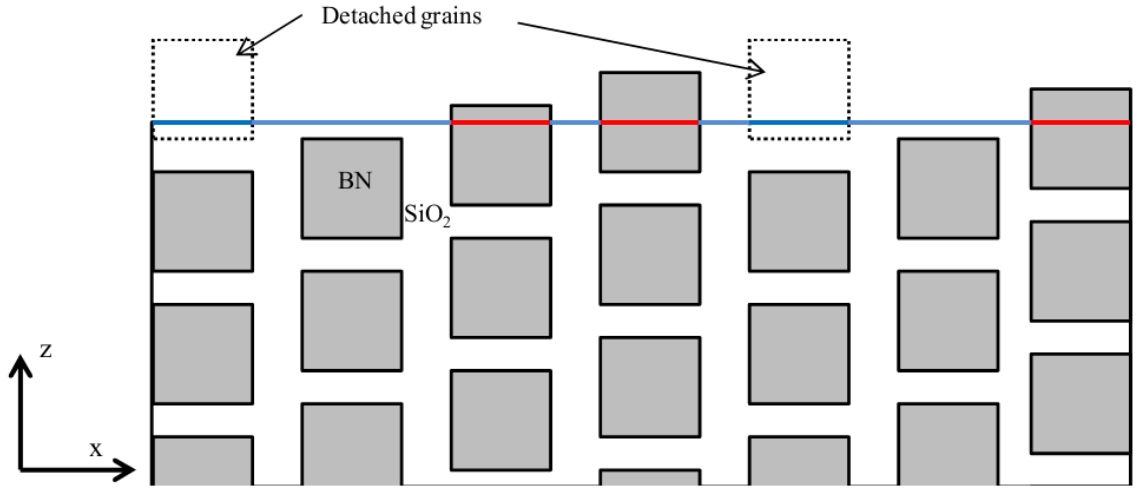

Figure 22. Composition changes due to ejection of grains with small support

In order to explain the variation in surface composition, another mechanism, such as the grain-ejection mechanism proposed above is needed. Atomic sputtering does not predict the decrease in BN in the highly-eroded region. Grain ejection provides a plausible mechanism that explains this surprising observation.

V. Conclusion

The modeling of atomic sputtering of a heterogeneous material is capable of reproducing some features observed experimentally in an eroded channel wall. The ridge and cliff structure to the surface is explained by BN, which has a lower sputtering rate, shadowing the silica material behind it. The surface features produced by the model are a strong function of the incidence angle of the ions. The observed ridge and cliff structures are similar to those produced by ions which impact at an angle of 30º. Experimental rms roughnesses in the eroded channel wall are similar to those produced by the model for incidence angles of 30º. This suggests that the plasma was impacting the P5 channel wall at a moderate angle of incidence. Variation in the modeled material composition produces variations in the average erosion rate, as expected. However, the average erosion rate deviates from what is expected from a simple law-of-mixtures, which demonstrates the significance of the surface structure and shadowing. Average erosion rates are biased towards those of the component with the lowest sputtering rate in the material mixture. The relative absence of BN in XPS measurements of the surface of a channel wall in the highly-eroded region remains unexplained, as this behavior is not captured in a pure atomic sputtering model. Theoretical reason to believe that sputtering cannot explain this behavior is presented. The ejection of BN grains with small support in the matrix is a plausible mechanism by which this surprising experimental variation in composition can be explained.

Acknowledgments

Prof Gregory Thompson and Thomas Burton of the University of Alabama for their SEM and XPS microscopy of the P5 channel wall, sample preparation work, and material science expertise.

References

[1]Hofer, R. Mikellides, I. Katz, I., "BPT-4000 Hall Thruster Discharge Chamber Erosion Model Comparison with Qualification Life Test Data," 30th *International Electric Propulsion Conference*, Florence, Italy, 2007.

[2]de Grys. Mathers. Welander., "Demonstration of 10,400 Hours of Operation on a 4.5 kW Qualification Model Hall Thruster," *AIAA Joint Propulsion Conference*, 2010-6698.

[3]Yim, John T., "Computational Modeling of Hall Thruster Channel Wall Erosion," PhD Thesis, University of Michigan, 2008.

[4]Zhang J. et al., "Sputtering investigation of boron nitride with secondary ion and secondary neutral mass spectrometry," *J. Vac. Sci. Tech*, A 15 (2) 243-247, 1997.

[5]Zidar D. Rovey L., "Hall-effect Thruster Channel Surface Properties Investigation (Preprint)," For publication, *AIAA Journal of Propulsion and Power*, AFRL-RZ-ED-JA-2011-056, March 2011.

[6]Zidar D. Rovey L., "Boron Nitride Hall-effect Thruster Channel Surface Properties Investigation," *AIAA Joint Propulsion Conference*. AIAA 2011-5993. 2011.

[7]Yalin, A. P., Rubin, B., Domingue, S. R., Glueckert, Z., and Williams, J. D., "Differential Sputter Yields of Boron Nitride, Quartz, and Kapton Due to Low Energy Xe+ Bombardment," *AIAA Paper 2007-5314*, July 2007.

[8]Garnier, Y. Viel, V. Roussel, J. F. and Bernard, J., "Low-Energy Xenon Ion Sputtering of Ceramics Investigated for Stationary Plasma Thrusters," *Journal of Vacuum Science and Technology*, A 17. 6. 3246-3254 (1999).

[9]Garnier Y. Viel V. Roussel J. "Investigation of Xenon Ion Sputtering of One Ceramic Material Used in SPT Discharge Chamber". *IEPC*. 1999.

[10]SRIM, Stopping Range of Ions in Matter (2008), Software Package, Ziegler, J. F.

[11]Haas, James M., "Low-Perturbation Interrogation of the Internal and Near-Field Plasma Structure of a Hall Thruster Using a High-Speed Probe Positioning System," PhD Thesis, University of Michigan, 2001.

[12]Gulczinski, Frank S., "Examination of the Structure and Evolution of Ion Energy Properties of a 5 kW Class Laboratory Hall Effect Thruster at Various Operational Conditions," PhD Thesis, University of Michigan, 1999.

[13]Sengupta, A. Brophy, J., "Status of the extended life test of the deep space 1 flight spare ion engine after 30,352 hours of operation," Jet Propulsion Laboratory, California Institute of Technology, Pasadena California, AIAA-2003-4558.

[14]M. Gamero-Castano, I. Katz., "Estimation of Hall Thruster Erosion Using HPHall," IEPC 2005-303, 29th IEPC, 21 Oct 2005.

[15]Smith, Timothy B. "Deconvolution of Ion Velocity Distributions from Laser-Induced Fluorescence Spectra of Xenon Electrostatic Thruster Plumes." PhD Thesis, University of Michigan. 2003.